JOURNAL OF GEOPHYSICAL RESEARCH, VOL. 100, NO. D5, PAGES 9007–9016, MAY 20, 1995

Transport of the Pinatubo volcanic aerosol to a northern midlatitude site

A. O. Langford, T. J. O'Leary,[1] and M. H. Proffitt,[1]
Aeronomy Laboratory, National Oceanic and Atmospheric Administration, Boulder, Colorado

M. H. Hitchman
Department of Atmospheric and Oceanic Sciences, University of Wisconsin, Madison

Abstract. A 2-year time series of high resolution lidar backscatter profiles at 0.532 μm, taken at the NOAA Fritz Peak Observatory (39.9°N, 105.3°W) is analyzed to investigate the evolution of the stratospheric aerosol following the eruption of Mount Pinatubo in June, 1991. Aerosol from the eruption first appeared as transient layers just above the tropopause in late summer and early fall of 1991. This was followed by a rapid increase in aerosol centered near 21 km, with an exponential risetime of ~22 days. The maximum in late December 1991 was followed by a slow decline, punctuated by seasonal increases below 18 km and with an exponential decay timescale of ~300 days near 20 km. Aerosol backscatter is converted to mass and a principal component analysis (PCA) is performed to explore the statistical properties of aerosol variability. More than 80% of the variability in aerosol mass is described by only three components, corresponding to variations in the layers 17-22 km (PC1, 44%), below 17 km (PC2, 27%), and above 22 km (PC3, 9%). Since most of the temporal variations occur independently in these three layers, this work provides further insight into the nature of stratospheric transport from the tropics to midlatitudes.

Introduction

The cataclysmic eruption of Mount Pinatubo (15.14°N, 120.35°E) in June 1991 ejected 12-15 million metric tons (Mt) of SO_2 into the atmosphere [*McPeters,* 1993] and led to a large increase in the sulfate aerosol burden of the stratosphere. The impact of this event on the atmosphere is still being evaluated. Potential radiative effects include surface cooling [*Lacis et al.,* 1992], altered photolysis rates [*Perliski and Solomon,* 1992], and changes in circulation patterns [*Kinne et al.,* 1992; *Labitzke and McCormick,* 1992; *Pitari,* 1993; *Kodera,* 1994] due to scattering and absorption of incoming solar radiation and trapping of outgoing infrared radiation by the aerosol particles. The sulfuric acid/water droplets that compose the aerosol can also act as condensation nuclei as they enter the upper troposphere, thereby affecting cloud formation and precipitation patterns [*Jensen and Toon,* 1992; *Sassen,* 1992; *Twomey,* 1991]. Finally, the particles can act as catalytic surfaces for heterogeneous processes that may increase the rate of ozone destruction in chlorine-dominated loss regimes. [*Hofmann,* 1987; *Hofmann and Solomon,* 1989; *Jäger and Wege* 1990; *Granier and Brasseur,* 1992; *Johnston et al.,* 1992; *Prather,* 1992; *Mills et al.,* 1993; *Hofmann et al.,* 1994].

Theoretical descriptions of the above processes rely on observations of the horizontal and vertical distribution and composition of the aerosol. Descriptions of the transport from the source region in the tropics to higher latitudes can also be used to evaluate stratospheric transport and general circulation models [e.g., *Boville et al.,* 1991]. A wealth of information about the evolution of the Pinatubo aerosol cloud is available from a variety of complementary ground based, in situ, and satellite based observations [*McCormick,* 1992]. Ground based lidar measurements [*DeFoor et al.,* 1992; *Jäger,* 1992] provide high spatial and temporal coverage of the aerosol distribution at a single location. In situ measurements [*Deshler et al.,* 1993, *Brock et al.,* 1993] provide information about the chemical and physical composition of the aerosol. Satellite measurements provide wide spatial coverage and have proven especially useful for describing the initial dispersion and transformation of the SO_2 gas cloud [*Bluth et al.,* 1992] and the resultant aerosol [*McCormick and Veiga,* 1992; *Stowe et al.,* 1992]. *Trepte and Hitchman* [1992] and *Trepte et al.* [1993] recently described the use of Stratospheric Aerosol and Gas Experiment (SAGE) I and II aerosol extinction data to infer stratospheric transport from tropical eruptions including El Chichón and Mount Pinatubo. These studies suggest that the aerosol is largely confined to a "tropical reservoir" in the lower stratosphere between 20°S and 20°N from which it is chronically transported poleward and downward in a "lower regime" and lofted over the tropics in an "upper regime." The climatological view taken by *Hitchman et al.* [1994] shows the integrated effect of all motions on the aerosol distribution, while *Trepte et al.* [1993] highlight the discrete-layered, advective nature of synoptic transport events. Here we attempt to provide useful information about this complex transport

[1]Also at Cooperative Institute for Research in Environmental Sciences, University of Colorado, Boulder.

Paper number 95JD00384.
0148-0227/95/95JD-00384$05.00

from a principal components analysis of time-altitude aerosol variations determined by lidar. Section 2 describes the lidar apparatus at the NOAA Aeronomy Laboratory Fritz Peak Observatory (FPO) (39.9°N, 105.3°W). The time-altitude variation of aerosol backscatter at 0.532 μm is described in section 3, with emphasis on the differing evolution with altitude. Section 4 describes the conversion to aerosol mass and the use of principal component analysis (PCA). Implications for the general circulation and aerosol transport are discussed in section 5.

Lidar Apparatus and Data Reduction

Fritz Peak Observatory is located at an elevation of 2.7 km in the Colorado mountains ~35 km northwest of Denver. The backscatter measurements were made using the 0.532-μm output of a frequency doubled Nd:YAG laser (November 1991 to June 1993) or the ~0.590-μm output of a Nd:YAG pumped dye laser (August 1991 to July 1992). For the present analysis the dye laser measurements made between August and November 1991 have been converted to 0.532-μm values using factors derived from simultaneous measurements. The unexpanded laser beams (~0.5 mrad full-width divergence) are directed upward and the backscattered radiation collected with a vertically pointing 61 cm f/1.8 telescope and imaged by a field lens onto the photocathode of an S-20 photomultiplier tube. The receiver field of view is typically set to ~1.8 mrad by a field stop placed at the prime focus. Interference filters are generally unnecessary for nighttime backscatter measurements at this location. The outgoing laser beams are displaced from the telescope axis by 1.2 m and the photomultiplier tube gated off for 25 to 35 μs after the laser fires to prevent detector saturation by the more intense Rayleigh scattering in the first 5-6 km. The photomultiplier bias is maintained at a sufficiently low level that the peak anode current does not exceed an empirically determined threshold where afterpulsing becomes significant. The signal is amplified by a 5-MHz current-to-voltage preamplifier followed by a 1-MHz voltage amplifier, digitized (12 bit, 10-MHz, 8192 channels), and averaged for 3.4 min (4096 laser shots) to obtain profiles with a vertical resolution of ~50 m.

The lidar equation describing the backscattered return signal for a laser with output power P_0 at wavelength λ can be written to give [*Russell et al.*, 1979; *Reagan et al.*, 1989]

$$ß(\lambda,z) = X(z)/CT^2(z) \quad (1)$$

where $ß(\lambda,z)$ is the elastic backscattering coefficient, $X(\lambda,z) = P(\lambda,z)z^2/P_0(\lambda)$ is the pulse and range normalized return power received at time $t = 2z/c$ after the laser pulse, C is a constant determined by the collection efficiency of the detection system, and $T^2(z) = \exp(-2\int_{0\rightarrow z}\alpha(r))dr$ is the round-trip transmittance from the laser to range z, with $\alpha(\lambda,z)$ the extinction coefficient due to scattering and absorption. The backscattering and extinction coefficients include contributions from both aerosol (Mie) $ß_a(\lambda,z)$ and molecular (Rayleigh) $ß_R(\lambda,z)$ scatterers, with the backscatter ratio $R(\lambda,z)$ defined as the ratio of total backscatter to molecular backscatter:

$$R(\lambda,z) = \{ß_a(\lambda,z)+ß_R(\lambda,z)\}/ß_R(\lambda,z) = 1+ß_a(\lambda,z)/ß_R(\lambda,z) \quad (2)$$

The backscatter ratio profile is calculated using a procedure based on the method of *Russell et al.* [1979] wherein the equation

$$R(\lambda,z) = \{X(z)ß_R(\lambda,z)T^2(z_0)R(z_0)\}/\{X(z_0)ß_R(\lambda,z_0)T^2(z)\} \quad (3)$$

is numerically solved from a starting range z_0, which is usually between 8 and 12 km, to a final range z_1 between 35 and 40 km. The partial transmission from z_0 to z (i.e., $T^2(z_0)/T^2(z)$) is iteratively calculated using Rayleigh and ozone extinction terms derived from the U.S. Standard Atmosphere (1976) and an aerosol extinction term calculated from an extinction-to-backscatter ratio $S = \alpha_a(\lambda,z)/ß_a(\lambda,z)$ taken from the model of *Jäger and Hofmann* [1991]. The ozone extinction term at 0.532 nm is generally negligible. The value of S is assumed to be independent of altitude for the calculations. Errors introduced by this assumption should be <5%. The profiles are normalized to give $R(z_1) = 1.0$ so that the initial value of $R(z_0)$ is constrained (to a value ≥1.0) for a given value of S. Alternatively, a check on the value of S is obtained when it can be safely assumed that $R(z_0) = 1.0$. Examination of the return signals suggests that the latter assumption is generally inappropriate. Profiles of the aerosol (Mie) elastic backscatter coefficient or cross section per unit volume, $ß_a(\lambda,z)$, in units of m^{-1} sr^{-1} are simultaneously calculated.

The major sources of error in the lidar measurements are differences between the actual molecular density profile and the U. S. Standard Atmosphere; the assumption that $S = \alpha_a(\lambda,z)/ß_a(\lambda,z)$ is known and invariant with altitude; and the assumption that $R(z_1) = 1.0$. Low signal to noise is generally not a problem below ~40 km unless a strongly attenuating cloud is present. For the relatively strong backscatter signals present during the measurement period, the combined errors are estimated to be ≤15%.

Time-Altitude Evolution of Aerosol Backscatter

The eruption of Mount Pinatubo occurred at a time when the stratospheric aerosol layer was approaching background levels [*DeFoor et al.*, 1992; *Jäger*, 1992] and significantly increased the aerosol loading in the lower stratosphere. The only other significant sources of stratospheric aerosols during the study period were the eruptions of Mount Spurr near Anchorage, Alaska in June, August, and September 1992. These eruptions were relatively minor, however, and ejected only ~0.7 Mton of SO_2 into the upper troposphere and lower stratosphere or only ~5% of the Mount Pinatubo output [*McClellan et al.*, 1992]. Thus the time evolution of the backscatter profile can provide considerable insight into the transport of the aerosol from the tropics to northern midlatitudes.

Figure 1 shows a smoothed contour plot of the 0.532-μm non-Rayleigh backscatter above FPO between August 9, 1991 (55 days after the main Pinatubo eruption on June 15) and June 13, 1993. The plot was constructed by grouping more than 120 backscatter profiles truncated at 12 km above mean sea level (ASL) into monthly averages with 0.5-km vertical resolution. The lowest contour level (5×10^{-8} m^{-1} sr^{-1}) is roughly twice the peak pre-Pinatubo level estimated from NOAA Environmental Technology Laboratory (ETL) (formerly Wave Propagation Laboratory (WPL)) ruby lidar measurements in Boulder during early 1991 [*Post et al.*, 1992]. The backscatter reached a maximum near 21 km in early December or 6 months after the eruption that was more than 10 times the peak pre-Pinatubo level. The altitude of the peak backscatter

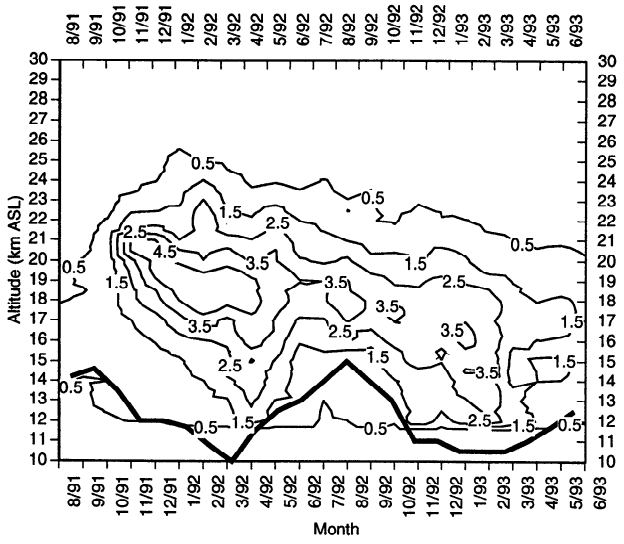

Figure 1. Contour plot of the aerosol backscatter cross section at 0.532-μm above Fritz Peak Observatory (39.9°N, 105.3°W). The plot is created from profiles acquired during 128 observing sessions between August 9, 1991, and June 22, 1993. The profiles are truncated at 12 km, averaged by month, and binned into 0.5-km intervals. The solid curve shows the tropopause height as determined from Denver radiosondes.

subsequently descended to nearly 16 km over the next 12 months due to sedimentation and descent. Midlatitude descent is expected as part of the Brewer-Dobson circulation [*Brewer,* 1949; *Dobson,* 1956; *Dunkerton,* 1978; *Holton,* 1981, 1986; *Solomon et al.,* 1986]. The maximum altitude with ß ≥ 5 x 10^{-8} m^{-1} sr^{-1} (i.e. the 0.5 contour level in Figure 1) decreased from ~25 km to nearly 20 km in the 18 months from January 1991 to June 1993. Large seasonal changes in the amount of backscatter in the lower stratosphere correlate inversely with changes in the Denver radiosonde tropopause height shown by the thick solid curve.

Figures 2a and 2b show the column-integrated backscatter between 12 and 30 km resolved into three altitude ranges: 12-17, 17-23, and 23-30 km. These intervals are based on the principal component analysis described below. A three-point boxcar smoothing has been applied to the data in Figure 2a for clarity. Figure 2b shows the (unsmoothed) observations during the first few months following the eruption. These have been supplemented by values extrapolated from measurements by the NOAA ETL 0.694-μm ruby lidar (C.J. Grund, personal communication, 1992) and a 0.589-μm dye laser lidar operated by Colorado State University ~75 km to the north in Fort Collins, Colorado [*Chen et al.,* 1992]. Appropriate conversion factors were derived from simultaneous measurements by the FPO and NOAA ETL lidars [*Post et al.,* 1992].

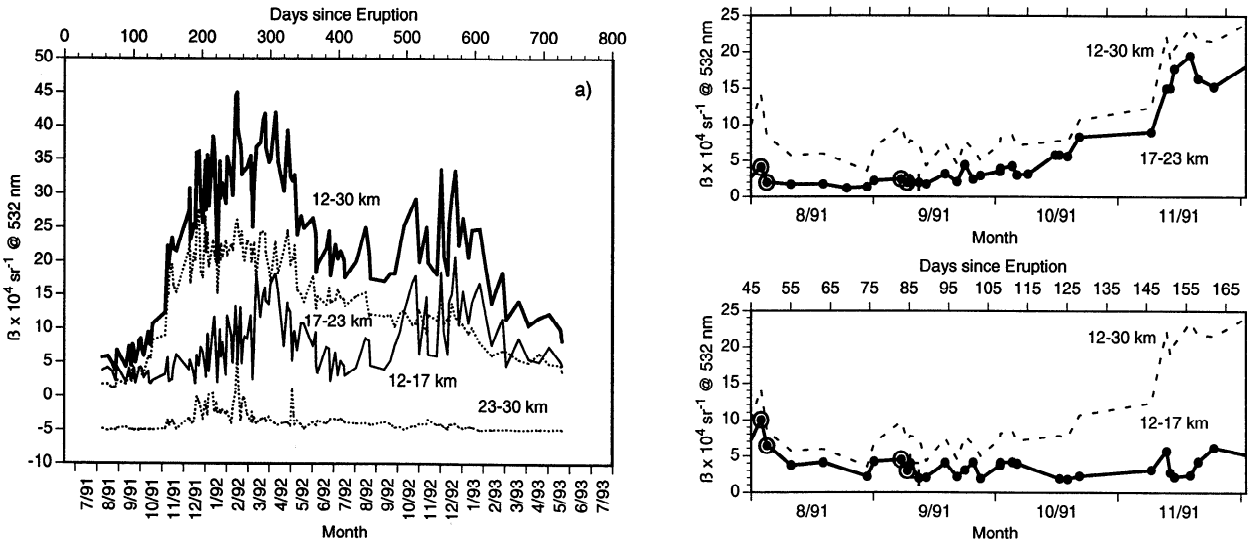

Figure 2. Evolution of the integrated aerosol backscatter cross section between 12 and 17 km, 17 and 23 km, 23 and 30 km, and 12 and 30 km. (a) Smoothed (three-point running mean) 0.532-μm Fritz Peak Observatory (FPO) lidar backscatter from August 9, 1991, to June 22, 1992. The observation frequency is indicated by the large points on the 12-to-30-km column backscatter. The data in the 23-30 km range are offset for clarity. (b) Unsmoothed 0.532-μm integrated backscatter from the FPO lidar with extrapolated values from the (⊙) NOAA Environmental Technologies Laboratory (ETL) ruby [*Post et al.,* 1992; C.J. Grund, personal communication, 1992] and plus CSU dye laser lidars [*Chen et al.,* 1992] from early August and mid-September 1991. The column-integrated backscatter from 12 to 30 km is shown in each plot for comparison (dotted curve).

The first observation of enhanced backscatter over Colorado (*Post et al.,* [1992], not shown) was on June 26, only 10 days after the Mount Pinatubo eruption and 45 days before the first observations at FPO. A transient layer was detected between 15 and 16 km by both the NOAA ETL coherent CO_2 Doppler [*Post,* 1986; *Post and Cupp* 1990] and the ruby [*Eberhard and McNice,* 1986] lidars. Enhanced backscatter was not detected again until July 27 but was present in all profiles subsequent to that date. A strong layer appeared at 22 km on August 2 but disappeared prior to the initial observations at FPO one week later. Initial FPO profiles showed a broad layer between the tropopause (~14 km) and 18 km with two narrow maxima between 18 and 20 km. In comparison, the asynchronous satellite maps of 1-μm extinction during late June through early August [*Trepte et al.,* 1993, Plates 2 and 3] suggest that tropical aerosol reached Colorado during the summer near 19 km but not near 24 km. During the summer, subtropical anticyclones can tap the tropical reservoir in discrete events, advecting material into the extratropics. Similar transport events below 20 km were documented above Japan in late June [*Hayashida and Sasano,* 1993] and Germany in early July [*Jäger,* 1992]. The large temporal variability of backscatter at lower levels is consistent with the discrete nature of these events. This vertical difference in behavior was also found in the general circulation simulations of *Boville et al.* [1991], where substantial transport to northern extratropics occurred during northern summer below 20 km; but above 20 km, there was a lack of transport until the transition to westerlies in the fall.

During the next few months the backscatter below 17 km generally declined while the backscatter between 17 and 23 km increased slowly. Most observations showed sharp layers that appeared in this region for only a few days. The backscatter above ~22 km remained quite low except for the transient layer in early August and another in early September (Figure 2b). The backscatter between 17 and 23 km increased sharply in mid-October to a maximum in late December. This was followed by a slow decline through the end of the measurement period. Significant backscatter did not consistently appear above 22 km until November. Measurable backscatter as high as 28 to 32 km was frequently observed in December, January, and February. The column-integrated backscatter generally increased through the beginning of April 1992, remained roughly constant during the summer, and then increased markedly in the lower stratosphere for a period of several months beginning in October 1992. The wintertime increases below 17 km coupled with the lack of a corresponding decrease at higher altitudes support the notion of enhanced poleward and downward transport during the northern winter and is consistent with a summertime reduction due, in part, to the effects of tropospheric convection. *Jäger and Carnuth* [1987] observed similar behavior following the eruption of El Chichón and *Hofmann and Rosen* [1987] concluded that these seasonal increases were due to enhanced advection of large (≥0.25 μm) particles. By June 1993 the column backscatter had declined to ~25% of the maximum value in January 1992, or about the same level as in early October 1991. Several thin transient layers that appeared below 17 km in August and September 1992 [*McClellan et al.,* 1992] may be due to the eruptions of Mount Spurr. These relatively sharp short-lived layers appeared to be to be superimposed on the larger Mount Pinatubo aerosol layers and contributed little to the integrated backscatter.

Principal Component Analysis of Aerosol Mass

A detailed description of transport using the backscatter data is hampered by the dependence of the lidar return on both the amount of particulate matter and the scattering efficiency of the particles. The latter depends on the particle size distribution and composition and thus changes with time. To better identify the influence of different processes on the aerosol profiles over FPO, the backscatter data have been converted to aerosol mass M, a more conservative tracer, and analyzed using principal component analysis (PCA).

The relationship between elastic backscatter and aerosol mass has been examined by several workers [e.g., *Pinnick et al.,* 1980; *Rosen and Hofmann,* 1986]. *Jäger and Hofmann* [1991] used in situ dustsonde measurements and Mie scattering calculations to derive 0.532-μm backscatter-to-mass conversion factors for the altitude ranges 15-20, 20-25, and 25-30 km between 1980 and 1987. This study showed that the value of M/ß for the region between 15 and 25 km decreased by ~25-35% following the eruption of El Chichòn in 1982. A similar analysis [*Jäger,* 1994] for the period from March 1991 to February 1994 shows comparable changes in M/ß following the eruption of Mount Pinatubo. The conversion factors of *Jäger et al.* [1994] are also in good agreement with those derived using multi-wavelength SAGE II data between October and December 1991 [*Thomason and Osborn,* 1992] and airborne measurements in the 15- to 21-km altitude range between August 1991 and March 1992 [*Brock et al.,* 1993]. The altitude dependent factors of *Jäger et al.* [1994] were used for the conversion process.

Principal component analysis or PCA (also known as eigenvector analysis and closely related to empirical orthogonal function analysis) performs an eigenvalue-eigenvector analysis of a matrix containing m observations of n variables to identify patterns of variances and covariances between the original variables. The principal components are then simply the eigenvectors of the variance-covariance matrix. Although originally developed as a psychometric technique, PCA has been widely used to examine the spatial and temporal variability of meteorological parameters [*Horel,* 1981] and the spatial distribution and sources of atmospheric pollutants [*Ashbaugh et al.,* 1984; *Buhr et al.,* 1992]. While most atmospheric applications have been concerned with time series of multicomponent measurements at a single point or horizontally dispersed measurements (i.e., on the ground or particular pressure surfaces) of a single quantity, the technique is also suited for the analysis of time series of vertical profiles [*Alexander et al.,* 1993].

Details of PCA are given in several texts [*Harman,* 1976; *Davis,* 1986; *Joliffe,* 1986; *Preisendorfer,* 1988]. For a series of m measurements of n variables the analysis is equivalent to rotating the original coordinate axes in n-dimensional space to a new reference frame where the axes correspond to the principal components or eigenvectors of the variance-covariance or correlation matrix. The first principal component extracted accounts for the most of the variance in the data, the second most of the remaining variance and so on. Since the principal components are linear combinations of the original variables weighted by the correlation coefficient or loading, the total number of components required to explain all of the variance is equal to the original number of variables. However, most of the variance can usually be explained by a

Table 1. Results of Principal Component Analysis

Component	Eigenvalue	Variance	Variance (rotated)
1	(5.316)	(0.443)	(0.27)
2	(3.273)	(0.273)	(0.331)
3	(1.095)	(0.091)	(0.206)
4	0.86	0.072	
5	0.485	0.04	
6	0.281	0.023	
Total	11.31	0.942	0.807

Eigenvalues considered significant are shown in parantheses.

much smaller number of principal components if the variables are correlated. Once the principal components are extracted, a second variance maximizing or varimax rotation [*Joliffe*, 1986] can be made using only the most significant components to align the new axes along the clusters of data, thereby simplifying the structure of the solution. This rotation changes the relative contributions of the previously identified components to the explained variance but does not explain any more of the original variance. Although the orthogonality constraint is sometimes relaxed in the varimax rotation, it is retained in the present analysis. It should be noted that while the principal components remain spatially orthogonal, they can vary independently with time.

To perform the analysis, profiles of the aerosol mass calculated from backscatter profiles obtained at FPO between 0100 and 0800 UT on 108 different nights were divided into twelve 1-km wide altitude bins from 13±0.5 to 24±0.5 km. The irregular spacing of the profiles does not lead to complications when the analysis is done in the time domain. Data from lower altitudes were excluded from the analysis because of possible contamination by cirrus clouds (profiles from nights with cirrus above 12 km were also identified through depolarization measurements and excluded from the analysis). The upper limit of 24 km was defined by excluding those altitudes where the mean backscatter is ≤20% of that at 19 km. Table 1 lists the eigenvalues and proportionate variance contributions obtained from the principal component analysis. More than 80% of the variance in the aerosol mass between 13 and 24 km during the 2 years following the eruption is described by only three principal components. Only these factors are retained for the varimax rotation.

Although principal component analysis helps to identify the number of processes responsible for most of the variance in the aerosol mass profiles, it provides no information about the associated physical mechanisms. This must be inferred with the aid of other information including the spatial and temporal dependence of the principal component loadings and scores. The loadings (correlation coefficients) for the rotated principal component are listed in Table 2 and plotted as a function of altitude in Figure 3. The communality gives the fraction of the variance at each altitude explained by the three components retained in the rotation. Following the analysis of *Heidam* [1982], only those loadings larger than 3 standard deviations are considered statistically significant; these are shown in parentheses in Table 2. The varimax rotation reveals a "simple structure" solution (i.e., loadings near 0 or 1) at most altitudes. PC1 explains most of the variance near the aerosol peak while PC2 and PC3 dominate the variance below 17 and above 23 km, respectively. The behavior of the aerosol at 19 km is almost completely uncorrelated with that below 17 and above 22 km.

Since the converted mass profiles should be relatively insensitive to microphysical processes such as condensation and coagulation, the vertical distribution should depend primarily on quasi-horizontal advection and diffusion and gravitational sedimentation. None of the rotated components exhibit an altitude dependence with large negative loadings at

Table 2. Rotated Component Loadings and Communalities

Altitude, km SL	PC1	PC2	PC3	Communality	3σ
13	-0.09	(0.80)	-0.01	0.652	0.59
14	-0.00	(0.90)	-0.06	0.813	0.43
15	0.05	(0.92)	-0.03	0.85	0.39
16	0.07	(0.88)	0.09	0.781	0.47
17	0.28	(0.74)	0.26	0.696	0.55
18	(0.63)	(0.50)	0.38	0.787	0.46
19	(0.82)	0.29	0.34	0.872	0.36
20	(0.92)	0.08	0.21	0.897	0.32
21	(0.85)	-0.10	0.11	0.746	0.50
22	(0.61)	0.03	(0.63)	0.762	0.49
23	(0.34)	0.03	(0.90)	0.918	0.29
24	0.17	0.03	(0.94)	0.911	0.30

Loadings considered significant are shown in parentheses.

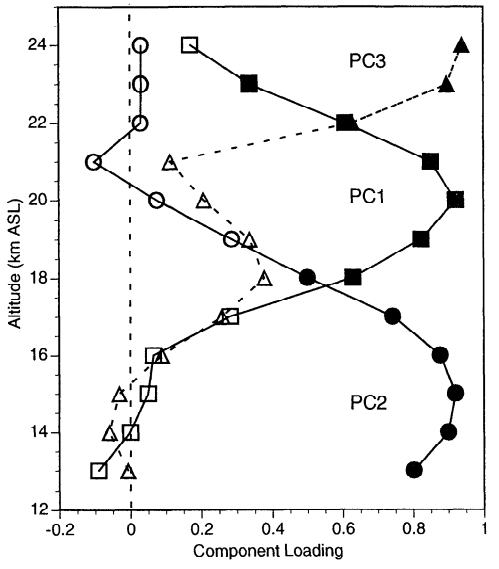

Figure 3. Loadings (correlation coefficients) from the orthogonal varimax transformation of the three significant principal components plotted as a function of altitude. Solid symbols represent those loadings considered statistically significant.

high altitudes and large positive loadings at low altitudes suggestive of net downward motion due to gravitational sedimentation (sedimentation would increase the aerosol at low altitudes relative to that at high altitudes). This is not too surprising since the PCA identifies the major sources of variance and thus is relatively insensitive to processes that are not apparent on short timescales. Thus we conclude that the first three components correspond primarily to quasi-horizontal large-scale transport processes. It is important to note that the magnitudes of the eigenvalues reflect only the contribution of each component to the variance and not the relative importance of the associated physical processes. However, the strong loading of each PC on distinct altitude ranges means that the relative importance can be estimated from the total integrated mass observed in those ranges. From this we infer that the processes corresponding to PC1, PC2, and PC3 are responsible for ≈50, 40, and 10%, respectively, of the total aerosol transport to 40°N.

The standardized scores for the rotated principal components are plotted as a function of time in Figure 4. The vertical axes show the contribution of each component to the individual profiles as standard deviations from the mean variance due to that component. Since the three components are spatially orthogonal, the scores can vary independently. Not surprizingly, the temporal evolution of the scores resembles that of the integrated backscatter in the corresponding altitude ranges of Figure 2a. PC1, which represents most of the aerosol mass, increases exponentially through the fall reaching a maximum at the first of the year ~200 days after the eruption. This is followed by an exponential decline through the end of the data record in June 1993. PC2 is much more variable, exhibiting a strong seasonal dependence, with maxima in the late winter of both years. PC2 also shows an initial decrease during the fall of 1991 as the relative importance of PC1 grows. PC3 is extremely variable and is dominated by several transient events occurring between late December 1991 and mid-March 1992. An event near February 20 was particularly strong and dominated the profile during that period, leading to a corresponding dip in the score of PC1. This type of variability is consistent with discrete planetary Rossby wave transport events in the mid-stratosphere during winter, such as described by *Leovy et al.* [1985].

Discussion and Conclusions

The time-altitude sections of aerosol backscatter and the PCA of aerosol mass at FPO provide a unique view of the evolution of the debris from Mount Pinatubo. In this section we discuss some of the implications for transport, including the layered aspect, dynamical mechanisms in each layer, the influence of the QBO, and time scales for the overall evolution. The primary spatial domains of PC1, PC2, and PC3 correspond to the layers 17-22 km, below 17 km, and above 22 km, respectively. Thus PC1 and PC2 are consistent with the "lower transport regime" seen in Tungsten 185 data [*Reed and German,* 1965] and in the aerosol climatology of *Hitchman et al.* [1994]. The differing temporal evolution of PC1 and PC2 suggests, however, that it is useful to distinguish processes above and below 17 km in the extratropics. During fall, winter, and spring, synoptic disturbances, traveling in the lower stratospheric westerlies, can transport aerosol into the extratropics. During the northern summer, aerosol backscatter in the 12 to 17-km layer is much lower, and the percent variance captured by PC2 is correspondingly lower.

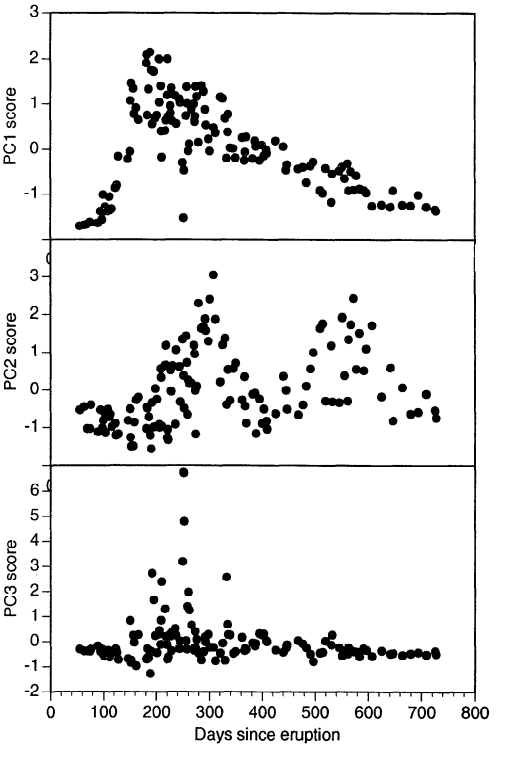

Figure 4. Principal component scores from the orthogonal varimax transformation plotted as a function of time. The scores are standard deviations from the mean contribution to the variance explained by that component.

The "tropopause" for zonal and seasonal mean aerosol near 40°N is near 8 km in winter but near 15 km in summer [*Hitchman et al.,* (1994), Figure 4]. Thus the summertime growth of the troposphere through convective activity exerts a strong seasonal influence on the lowest portion of the aerosol layer. Figure 1 suggests that a significant loss of stratospheric aerosol occurs by upward encroachment of the troposphere in the summer. Thus convective mixing is probably an important mechanism for the extratropical transport of mass from the stratosphere to the troposphere during summer.

Variability above 22 km, reflected in the weighting of PC3, is highest during the first winter, before sedimentation and the poleward-downward air motion led to a reduction in the mean altitude of the aerosol maximum. Variability in this regime is consistent with episodic planetary Rossby wave events. Variability in the intermediate layer (PC1) is much less than in the other layers. This layer is subject to transport processes that influence both the layer above and the layer below. Upwardly evanescent disturbances, such as summertime monsoon anticyclones, traveling synoptic Rossby waves, and inertiogravity waves can influence the lower and middle layer, while equatorward refracting planetary Rossby waves can influence the upper and middle layers [*Andrews et al.,* 1987]. Another factor is that the equatorial aerosol reservoir maximum is near 21 km, so that poleward and downward transport by layered advective processes, which occur at different levels at different times, would yield a maximum sustained transport in the ensemble for this middle layer. A further ingredient which would foster reduced variability in the intermediate layer is vertical mixing of discrete-layered tongues by gravity waves [e.g., *Iwasaki et al.,* 1989; *Danielsen et al.,* 1991; *Pfister et al.,* 1993] and other sloping smaller scale perturbations subjected to dissipative processes.

It is of interest to note that aerosol backscatter in the layer 12-17 km and the weighting of PC2 is fairly similar during the winters of 1991/1992 and 1992/1993, despite the overall removal of aerosol during the intervening year. In contrast, the aerosol backscatter above 22 km and the weighting of PC3 is quite small during the winter of 1992/1993 and values in the intermediate layer (PC1) show an almost monotonic decrease from January 1992. The magnitude of the increase suggests enhanced poleward transport from the tropics, although transport from higher latitudes cannot be ruled out through the present analysis. While sedimentation and subsidence are consistent with this overall trend, the quasi-bienniel oscillation (QBO) would be expected to amplify poleward transport enhancing the second-winter surge of aerosol at the lowest levels. Figure 5 shows monthly mean zonal winds over Singapore, where a climatological annual signal has been subtracted. The predominant sense of vertical shear of the zonal wind was easterly from the eruption of Mount Pinatubo through mid-1992, when descending westerly shear began to dominate. As shown by *Trepte and Hitchman* [1992] and *Hitchman et al.* [1994], aerosol is lofted over the equator during QBO easterly shear, favoring transport by planetary scale Rossby waves [e.g., *Hess and O'Sullivan,* 1994] in an "upper regime." This would promote variability in PC3 and help explain the surge seen in September 1991 in the top panel of Figure 2b. During QBO westerly shear, tropical confinement is reduced, with more aerosol available for transport poleward and downward in a "lower regime." Thus the descent of tropical westerly shear into the lower stratosphere during the winter of 1992/1993 would tend to promote poleward transport of aerosol to Colorado below 17 km. This would ultimately lead to a more rapid reduction of total stratospheric aerosol through venting of the tropical reservoir.

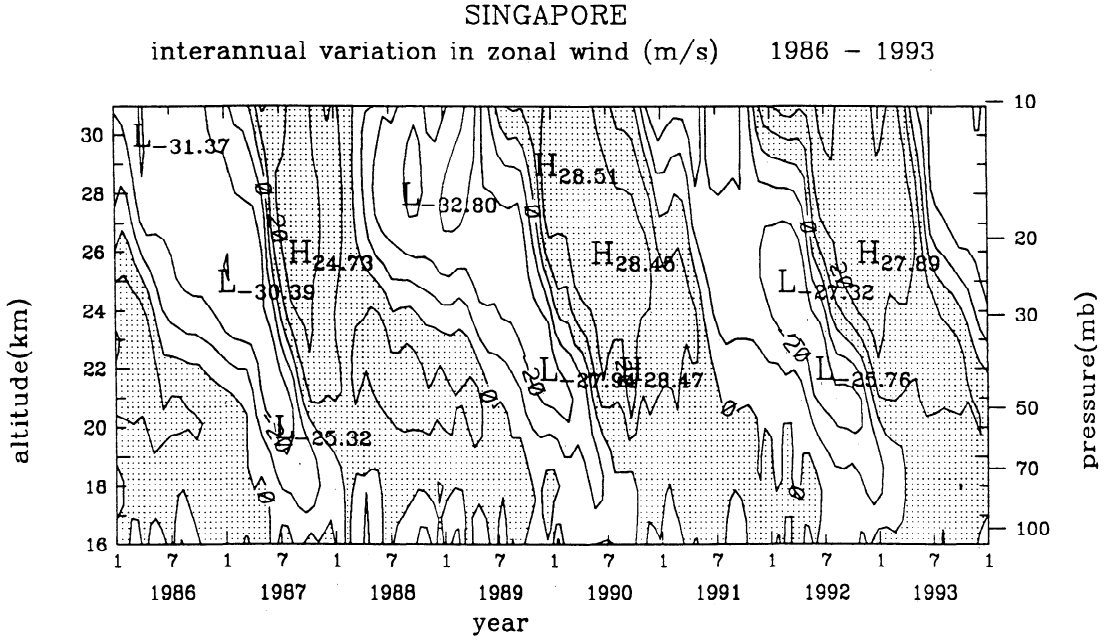

Figure 5. Time altitude cross sections of zonal winds from radiosonde profiles at Singapore (1°N, 104°E) illustrating the quasi-bienniel oscillation (QBO) during January 1988 to January 1994. A 35-year annual composite of monthly means has been subtracted from the monthly mean winds for this period. These data should be representative of the phase of the QBO but not actual winds at all longitudes. Westerly winds are stippled and the contour interval is 10 m s^{-1}.

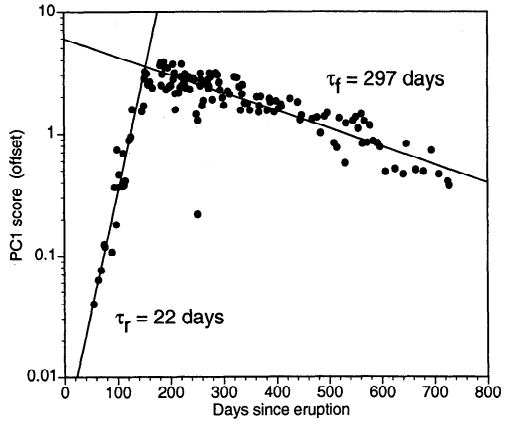

Figure 6. Principal component scores for PC1 with exponential least squares fit of the rise and fall portions of the curve. The 1/e time constants for the rise and fall are 22 and 297 days, respectively.

The primary characteristics of Figure 1 are captured by PC1. Figure 6 shows the evolution of PC1 scores replotted on an exponential scale. The rise and fall is approximated quite well by e-folding timescales of 22 and 300 days, respectively. Similar values are obtained by fitting the mass data near 20 km. Since the Pinatubo material was injected near 15° N, an effective meridional transport velocity to 40° N may be roughly estimated to be 1.5 m s^{-1} for the fall and winter of 1991. This is similar to values estimated from isochrones of arrival of radioactive material [*Feely and Spar,* 1960], the Bali eruption [*Dyer and Hicks,* 1968], stratospheric mass budgets [e.g., *Holton,* 1990], and stratospheric models [e.g., *Brasseur et al.,* 1990]. A crude estimate of an effective meridional diffusion coefficient, K_{yy}, may be made by dividing the square of the latitudinal separation by this e-folding risetime, yielding $K_{yy} \sim 4 \times 10^6$ m^2 s^{-1}. The 300-day decay time scale represents the gradual depletion of the tropical reservoir by poleward transport and entry of air into the troposphere. The decrease in the altitude of the maximum backscatter from ~21 to 17 km during 1992 suggests an effective extratropical descent velocity of about 0.014 cm s^{-1} (~4.5 km yr^{-1}) which is roughly twice the mean gravitational sedimentation velocity of ~0.007 cm s^{-1} (~2 km yr^{-1}) for a 0.3-μm-diameter H_2SO_4/H_2O particle with a density of 1.65 g cm^{-3} [*Kasten,* 1968].

In summary, our analysis of high-resolution lidar measurements at a midlatitude site during the first 2 years following the eruption of Mount Pinatubo is consistent with the concept of a tropical reservoir from which aerosol is transported poleward and downward, with modulation by season and phase of the QBO. Our results show that transport often occurs rather independently in the layers below 17 km, 17-22 km, and above 22 km. Much work still needs to be done to quantify specific dynamical contributions to this transport. Future plans include detailed case-study comparisons of parcel trajectory calculations with discrete events seen at FPO.

Acknowledgements. The authors would like to thank M.P. Buhr of the Aeronomy Laboratory for helpful discussions about principal component analysis. The authors would like to thank Joyce Yao of the University of Wisconsin for preparing the QBO time series. The encouragement and advice of Ed Danielsen of Sisters, Oregon, is gratefully acknowledged.

This work is supported as part of NOAA's Climate and Global Change Program.

References

Alexander, G. D., G .S. Young, and D. V. Ledvina, Principal component analysis of vertical profiles of Q1 and Q2 in the tropics, *Mon. Weather Rev., 121,* 535-548, 1993.

Andrews, D. G., J. R. Holton, and C. B. Leovy, *Middle atmosphere dynamics, first ed., vol. 40,* International geophysics series, Academic Press, Inc., edited by R. Dmowska and J. R. Holton, Orlando, Fl. 1987.

Ashbaugh, L. L., L. O. Myrup, and R. G. Flocchini, A principal component analysis of sulfur concentrations in the western United States, *Atmos. Environ., 18,* 783-791, 1984.

Bluth, G. J. S., S. D. Doiron, C. C. Schnetzler, A. J. Krueger, and L. S. Walter, Global tracking of the SO_2 clouds from the June 1991 Mount Pinatubo eruptions, *Geophys. Res. Lett., 19,* 151-154, 1992.

Boville, B. A., J. R. Holton, and P. W. Mote, Simulation of the Pinatubo aerosol cloud in general circulation model, *Geophys. Res. Lett., 18,* 2281-2284, 1991.

Brasseur, G., M. Hitchman, S. Walters, M. Dymek, E. Falise, and M. Pirre, An interactive chemical dynamical radiative two-dimensional model of the middle atmosphere, *J. Geophys. Res., 95,* 5639-5656, 1990.

Brewer, A. W., Evidence for a world circulation provided by the measurements of helium and water vapor distribution in the stratosphere, *Q. J. R. Meteorol. Soc., 75,* 351-363, 1949.

Brock, C. A., H. H. Jonsson, J. C. Wilson, J. E. Dye, D. Baumgardner, S. Borrman, M. C. Pitts, M. T. Osborn, R. J. DeCoursey, and D. C. Woods, Relationships between optical extinction, backscatter, and aerosol surface and volume in the stratosphere following the eruption of Mount Pinatubo, *Geophys. Res. Lett., 20,* 2555-2558, 1993.

Buhr, M. P., M. Trainer, D. D. Parrish, R. E. Sievers, and F. C. Fehsenfeld, Assessment of pollutant inventories by principal component analysis of ambient air measurements, *Geophys. Res. Lett., 19,* 1009-1012, 1992.

Chen, H., J. R. Yu, and C. Y. She, Arrival of Pinatubo disturbances in the stratospheric aerosol layer over Fort Collins, Colorado by a lidar at 589 nm, *Appl. Phys. B, 55,* 159-163, 1992.

Danielsen, E. F., R. S. Hipskind, W. L. Starr, J. F. Vedder, S. E. Gaines, D. Kley, and K. K. Kelly, Irreversible transport in the stratosphere by internal waves of short vertical wavelength, *J. Geophys. Res., 96,* 17,433-17,452, 1991.

Davis, J. C., *Statistics and Data Analysis in Geology,* New York, John Wiley, New York, 1986.

DeFoor, T. E., E. Robinson, and S. Ryan, Early lidar observations of the June 1991 Pinatubo eruption plume at Mauna Loa Observatory, Hawaii, *Geophys. Res. Lett., 19,* 187-190, 1992.

Deshler, T., B. J. Johnson, and W. R. Rozier, Balloonborne measurements of Pinatubo aerosol during 1991 and 1992 at 41°N: Vertical profiles, size distribution, and volatility, *Geophys. Res. Lett., 20,* 1435-1438, 1993.

Dobson, G. M. B., Origin and distribution of polyatomic molecules in the atmosphere, *Proc. R. Soc. London A, 236,* 187-192, 1956.

Dunkerton, T., On the mean meriodonal mass transport of the

stratosphere and mesosphere, *J. Atmos. Sci., 35,* 2325-2333, 1978.

Dyer, A. J. and B. Hicks, Global spread of volcanic dust from the Bali eruption of 1963, *Q. J. R. Meteorol. Soc., 94,* 545-554, 1968.

Eberhard, W. L. and G. T. McNice, Versatile lidar for atmospheric studies, including plume dispersion, clouds, and stratospheric aerosol, *J. Atmos. Oceanic Technol., 3,* 614-622, 1986.

Feely, H. W., and J. Spar, Tungsten-185 from nuclear bomb tests as a tracer for stratospheric meteorology, *Nature, 188,* 1062-1064, 1960.

Granier, C., and G. Brasseur, Impact of heterogeneous chemistry on model predictions of ozone changes, *J. Geophys. Res., 97,* 18,015-18,033, 1992.

Harman, H. H., *Modern Factor Analysis,* University of Chicago Press, Chicago, Ill., 1976.

Hayashida, S., and Y. Sasano, Stratospheric aerosol change in the early stage of volcanic disturbance by the Pinatubo eruption observed over Tsukuba, Japan, *Geophys. Res. Lett., 20,* 575-578, 1993.

Heidam, N. Z., Atmospheric aerosol factor models, mass and missing data, *Atmos. Environ., 16,* 1923-1931, 1982.

Hess, P. G., and D. O'Sullivan, A three dimensional modeling study of the extratropical quasi-bienniel oscillation in ozone, *J. Atmos. Sci.,* in press, 1995.

Hitchman, M. H., M. A. McKay, and C. R. Trepte, A climatology of stratospheric aerosol, *J. Geophys. Res., 99,* 20,689-20,700, 1994.

Hofmann, D. J., Perturbations to the global atmosphere associated with the El Chichon volcanic eruption of 1982, *Rev. Geophys., 25,* 743-759, 1987.

Hofmann, D. J. and J. M. Rosen, On the prolonged lifetime of the El Chichón sulfuric acid aerosol cloud, *J. Geophys. Res., 92,* 9,825-9,830, 1987.

Hofmann, D. and S. Solomon, Ozone destruction through heterogeneous chemistry following the eruption of El Chichón, *J. Geophys. Res., 94,* 5029-5041, 1989.

Hofmann, D. J., et al., Ozone loss in the lower stratosphere over the United States in 1992-1993: Evidence for heterogeneous chemistry on the Pinatubo aerosol., *Geophys. Res. Lett., 21,* 65-68, 1994.

Holton, J. R., An advective model for two-dimensional transport of stratospheric trace species., *J. Geophys. Res., 86,* 11,989-11,994, 1981.

Holton, J. R., Meridonal transport of stratospheric trace constituents, *J. Atmos. Sci., 43,* 1238-1242, 1986.

Holton, J. R., On the global exchange of mass between the stratosphere and troposphere, *J. Atmos. Sci., 47,* 392-395, 1990.

Horel, J. D., A rotated principal component analysis of the interannual variability of the northern hemispheric 500 mb height field, *Mon. Weather Rev., 109,* 2080-2092, 1981.

Iwasaki, T., S. Yamada, and K. Tada, A parameterization scheme of orographic gravity wave drag with two different vertical partitionings, II, Zonally averaged budget analyses based on the Eulerian mean method, *J. Meteorol. Soc. Jpn. 67,* 29-40, 1989.

Jäger, H., Pinatubo eruption cloud observed by lidar at Garmisch-Partenkirchen, *Geophys. Res. Lett., 19,* 191-194, 1992.

Jäger, H., and W. Carnuth, The decay of the El Chichón stratospheric perturbation observed by lidar at Garmisch-Partenkirchen, *Geophys. Res. Lett., 14,* 696-699, 1987.

Jäger, H., and D. Hofmann, Midlatitude lidar backscatter to mass, area, and extinction conversion model based on in situ aerosol measurements from 1980 to 1987, *Appl. Opt., 30,* 127-137, 1991.

Jäger, H., and K. Wege, Stratospheric ozone depletion at northern midlatitudes after major volcanic eruptions, *J. Atmos. Chem., 10,* 273-287, 1990.

Jäger, H., V. Freudenthaler, and F. Homburg. *Stratospheric aerosols and Pinatubo eruption clouds,* paper presented at the 17th International Conference on Laser Radar, pp. 371-374, Laser Radar Society of Japan, Sendai, Japan, 1994.

Jensen, E. J., and O. B. Toon, The potential effects of volcanic aerosols on cirrus cloud microphysics, *Geophys. Res. Lett., 19,* 1759-1762, 1992.

Johnston, P. V., R. L. McKenzie, J. G. Keys, and W. A. Matthews, Observations of depleted NO_2 following the Pinatubo volcanic eruption, *Geophys. Res. Lett., 19,* 211-213, 1992.

Joliffe, I. T., *Principal Component Analysis,* Springer-Verlag, New York, 1986.

Kasten, F., Falling speed of aerosol particles, *J. Appl. Meteorol., 7,* 944-947, 1968.

Kinne, S., O. B. Toon, and M. J. Prather, Buffering of stratospheric circulation by changing amounts of tropical ozone: A Pinatubo case study, *Geophys. Res. Lett., 19,* 1927-1930, 1992.

Kodera, K., Influence of volcanic eruptions on the troposphere through stratospheric dynamical processes in the northern hemisphere winter, *J. Geophys. Res., 99,* 1273-1282, 1994.

Labitzke, K., and M. P. McCormick, Stratospheric temperature increases due to Pinatubo aerosols, *Geophys. Res. Lett., 19,* 207-210, 1992.

Lacis, A. A., J. E. Hansen, and M. Sato, Climate forcing by stratospheric aerosols, *Geophys. Res. Lett., 19,* 1607-1610., 1992.

Leovy, C. B., and M. H. Hitchman, Dynamical phenomena in the equatorial middle atmosphere during northern winter 1978-1979, *Proceedings of the First National Workshop on the Global Weather Experiment, Current Achievements and Future Directions,* 2, pp. 581-591, National Academy Press, Washington, D. C., 1985.

McClellan, L., L. Schramm, J. Goldberg, E. Venzke, S. Stanisic (Eds.), Smithsonian Institution, *Bull. Global Volcanism Network, 17*(8), 1-2, 1992.

McCormick, M. P., Initial assessment of the stratospheric and climatic impact of the 1991 Mount Pinatubo eruption: Prologue, *Geophys. Res. Lett., 19,* 149, 1992.

McCormick, M. P., and R. E. Veiga, SAGE II measurements of early Pinatubo aerosols, *Geophys. Res. Lett., 19,* 155-158, 1992.

McPeters, R. D., The atmospheric SO_2 budget for Pinatubo derived from NOAA-11 SBUV/2 spectral data, *Geophys. Res. Lett., 20,* 1971-1974, 1993.

Mills, M. J., A. O. Langford, T. J. O'Leary, K. Arpag, H. L. Miller, M. H. Proffitt, R. W. Sanders, and S. Solomon, On the relationship between stratospheric aerosols and nitrogen dioxide, *Geophys. Res. Lett., 20,* 1187, 1993.

Perliski, L. M. and S. Soloman, Radiative influences of Pinatubo volcanic aerosols on twilight observations of

NO_2 column abundances, *Geophys. Res. Lett., 19,* 1923-1926, 1992.

Pfister, L., K. R. Chan, T. P. Bui, S. Bowen, M. Legg, B. Gary, K. Kelly, M. Proffitt, and W. Starr, Gravity waves generated by a tropical cyclone during the STEP tropical field program: A case study, *J. Geophys. Res., 98*, 8611-8638, 1993.

Pinnick, R. G., S. G. Jennings, and P. Chylek, Relationships between extinction, absorption, backscattering, and mass content of sulfuric acid aerosols, *J. Geophys. Res., 85,* 4059-4066, 1980.

Pitari, G., A numerical study of the possible perturbation of stratospheric dynamics due to Pinatubo aerosols: Implications for tracer transport, *J. Atmos. Sci., 50,* 2443-2461, 1993.

Post, M. J., Atmospheric purging of El Chichón debris, *J. Geophys. Res., 91,* 5222-5228, 1986.

Post, M. J., and R. E. Cupp, Optimizing a pulsed Doppler lidar, *Appl. Opt., 29,* 4145-4158, 1990.

Post, M. J., C. J. Grund, A. O. Langford, and M. H. Proffitt, Observations of Pinatubo ejecta over Boulder, Colorado by lidars of three different wavelengths, *Geophys. Res. Lett., 19,* 195-198, 1992.

Prather, M., Catastrophic loss of stratospheric ozone in dense volcanic clouds, *J. Geophys. Res., 97,* 10,187-10,191, 1992.

Preisendorfer, R. W., *Principal component analysis in meteorology and oceanography,* vol. 17, *Developments in atmospheric Science,* edited by C. D. Mobley, Elsevier, New York, 1988.

Reagan, J. A., M. P. McCormick, and J. D. Spinhirne, Lidar sensing of aerosols and clouds in the troposphere and stratosphere, Proc., *IEEE, 77,* 433-448, 1989.

Reed, R. J., and K. E. German, A contribution to the problem of stratospheric diffusion by large-scale mixing, *Mon. Weather Rev., 93,* 313-321, 1965.

Rosen, J. M., and D. J. Hofmann, Optical modeling of stratospheric aerosols: Present status, *Appl. Opt., 25,* 410-419, 1986.

Russell, P. B., T. J. Swissler, and M. P. McCormick, Methodology for error analysis and simulation of lidar aerosol measurements, *Appl. Opt., 18,* 3783-3797, 1979.

Sassen, K., Evidence for liquid-phase cirrus cloud formation from volcanic aerosols: Climatic implications, *Science, 257,* 516-519, 1992.

Solomon, S., J. T. Kiehl, R. R. Garcia, and W. Grose, Tracer transport by the diabatic circulation deduced from satellite observations, *J. Atmos. Sci., 43,* 1603-1617, 1986.

Stowe, L. L., R. M. Carey, and P. P. Pellegrono, Monitoring the Mount Pinatubo aerosol layer with NOAA/11 AVHRR data, *Geophys. Res. Lett., 19,* 159-162, 1992.

Thomason, L. W., and M. T. Osborn, Lidar conversion parameters derived from SAGE II extinction measurements, *Geophys. Res. Lett., 19,* 1655-1658, 1992.

Trepte, C. R., and M. H. Hitchman, Tropical stratospheric circulation deduced from satellite aerosol data, *Nature, 355,* 626-628, 1992.

Trepte, C. R., R. E. Veiga, and M. P. McCormick, The poleward dispersal of Mount Pinatubo volcanic aerosol, *J. Geophys. Res., 98,* 18,563-18,573, 1993.

Twomey, S., Aerosols, clouds and radiation, *Atmos. Environ., 25*(A), 2435-2442, 1991.

M. H. Hitchman, Department of Atmospheric and Oceanic Sciences, University of Wisconsin, 1225 West Dayton Street, Madison, WI 53706. (email: matt@adams.meteor.wisc.edu)

A. O. Langford, T. J. O'Leary, and M. H. Proffitt, NOAA Aeronomy Laboratory, 325 Broadway, R/E/AL6, Boulder, CO 80303. (email: langford@al.noaa.gov)

(Received May 10, 1994; revised January 13, 1995; accepted January 17, 1995.)